Materials Research Bulletin 171 (2024) 112631

Contents lists available at ScienceDirect

Materials Research Bulletin

journal homepage: www.elsevier.com/locate/matresbu

Research Papers

Interface and magnetic-dielectric synergy strategy to develop Fe_3O_4-Fe_2CO_3/multi-walled carbon nanotubes/reduced graphene oxide mixed-dimensional multicomponent nanocomposites for microwave absorption

Hemin Wang [a], Yanling Hao [b], Lele Xiang [a], Xiaosi Qi [a,*], Lei Wang [c], Junfei Ding [a], Yunpeng Qu [a], Jing Xu [a], Wei Zhong [d]

[a] College of Physics, Guizhou Province Key Laboratory for Photoelectrics Technology and Application, Guizhou University, Guiyang 550025, China
[b] Minzu Normal University of Xingyi, Xingyi 562400, China
[c] National Demonstration Center for Experimental Materials Science and Engineering Education Jiangsu University of Science and Technology, Zhenjiang 212003, China
[d] National Laboratory of Solid State Microstructures and Jiangsu Provincial Laboratory for NanoTechnology, Nanjing University, Nanjing 210093, China

ARTICLE INFO

Keywords:
Mixed-dimensional structure
Fe_3O_4-$FeCO_3$/MWCNTs/RGO multicomponent nanocomposites
Magnetic-dielectric synergistic effect
Interfacial engineering
Microwave absorption

ABSTRACT

Interfacial and/or magnetic-dielectric synergistic effects are important avenues to boost microwave absorption properties. In order to simultaneously utilize these effects, we elaborately designed mixed-dimensional Fe_3O_4-$FeCO_3$/multi-walled carbon nanotubes (MWCNTs)/reduced graphene oxide (RGO) multicomponent nanocomposites (MCNCs) in large scale via a facile process of hydrothermal and freeze-drying. The microstructural investigation revealed that two-dimensional RGO, one-dimensional MWCNTs and zero-dimensional Fe_3O_4-$FeCO_3$ nanoparticles were well bounded to generate the typical mixed-dimensional structure. By controlling the amounts of initial reactants, the Fe_3O_4-$FeCO_3$/MWCNTs/RGO MCNCs displayed improved impedance matching features, polarization and conduction loss abilities, which lead to the evidently improved electromagnetic absorption properties. The Fe_3O_4-$FeCO_3$/MWCNTs/RGO MCNCs simultaneously exhibited excellent absorption ability, large absorption bandwidth, low density and thin matching thickness. Generally, this work not only proposed an effective route to make the best of magnetic-dielectric synergy and interfacial strategy for exploiting novel microwave absorption materials, but also presented a simple approach to synthesize magnetic MWCNTs/RGO-based mixed-dimensional MCNCs.

1. Introduction

Owing to the abundant diversities in the composition and structure, multicomponent nanocomposites (MCNCs) exhibited much more extraordinary properties and promising application prospects compared to single-composition substances, which have attracted the intensive attention all the time [1–3]. Amongst, carbon-based MCNCs including graphene (G), carbon foams (CFs) and carbon nanotubes (CNTs) have always been the research hotspots owing to their unique structures, fascinating chemical and physical performances of carbon materials [4–6]. Meanwhile, the promising applications and gradually serious electromagnetic (EM) interference issues urgently required the researchers to exploit high-efficiency microwave absorbers (MAs), which have the characteristics of good absorption ability, broad absorption bandwidth, low density, thin thickness and excellent chemical stability [7–9]. According to the previous results and EM energy conversion principle [10,11], the magnetic-dielectric synergistic effect played a very important role in the EM wave absorption properties (EMWAPs). Therefore, different structures and categories of carbon-based MCNCs such as Co_xNi_y@C nanosheets [12], NiO/Ni@C [13], Ni/MXene/reduced G oxide (RGO) [14], $Ni_3ZnC_{0.7}$/CNTs/nano-porous carbon [15] have been developed. In general, the obtained results demonstrated that designing carbon-based magnetic MCNCs consisting of magnetic nanoparticles and carbon materials were a desirable way to develop the desirable candidates for high-efficiency MAs. And the magnetic-dielectric synergistic effect was high dependent on their EM

* Corresponding author.
E-mail address: xsqi@gzu.edu.cn (X. Qi).

https://doi.org/10.1016/j.materresbull.2023.112631
Received 25 September 2023; Received in revised form 14 November 2023; Accepted 21 November 2023
Available online 22 November 2023

parameters and impedance matching characteristic, which were determined by the microstructure and compositions [16,17]. To this end, the selective synthesis of carbon-based magnetic MCNCs with more tunable microstructural parameters should be a viable strategy to optimize their impedance matching characteristics and magnetic-dielectric synergistic effects.

Besides, interfacial effect was demonstrated to play an important role in the enhancement of EMWAPs [18–20]. And designing the abundant interfaces to strengthen the interface polarization is a good way to dissipate the EM waves in the high frequency region. Consequently, various structures and morphologies including core/shell, heterostructure and hollow were elaborately constructed and intensively investigated owing to the excellent interfacial and synergistic effects [21–23]. For instance, Che and his co-workers effectively used the unique interfacial property of hierarchical hollow structure to design the magnetized Fe_3O_4@$Ti_3C_2T_x$/CNTs microsphere. Benefiting from the abundant interfacial polarization, the obtained Fe_3O_4@$Ti_3C_2T_x$/CNTs exhibits the extraordinary comprehensive EMWAPs [24]. For effective utilizing the interfaces, Cao's group successively proposed a facile solvothermal/hydrothermal method to produce two-dimensional (2D)/2D WS_2-RGO and $MoSe_2$@RGO heterostructures. The results demonstrated that the excellent interfacial effect endowed their excellent multiple-interface scattering and interfacial dielectric coupling, which resulted in their outstanding EMWAPs [25,26]. To intelligently integrate multiple heterostructures for enhancing dielectric polarization, Wu et al. designed a targeted induction and vapor-phase selenization process to produce zero-dimensional (0D)@2D@one-dimensional (1D) hierarchical structures Co_xSe_y/NiSe@carbon nanosheets@carbon nanofibers. The results verified that the mixed-dimensional heterostructures greatly improved the impedance matching features and loss mechanisms, which endowed the extremely superior EMWAPs of designed composite fabric with the extremely low filling load [27]. Generally, the previous results demonstrated that constructing rich interfaces evidently strengthened the interface polarization and dissipation of EM waves. Therefore, mixed-dimensional MCNCs should be acted as the good candidates for high-performance MAs because of the excellent synergistic effects, abundant interfaces and compositions [28]. However, it is still very difficult to produce mixed-dimensional MCNCs in large scale, which extremely hinder the applications in microwave absorption.

Inspired by the above-mentioned viewpoints and our previous outcomes [29,30], herein, we presented a facile hydrothermal and freeze-drying process to synthesize mixed-dimensional Fe_3O_4-$FeCO_3$/-multi-walled carbon nanotubes (MWCNTs)/RGO MCNCs in high efficiency. By regulating the amount of hydroxylated MWCNTs and graphene oxide (GO), the obtained Fe_3O_4-$FeCO_3$/MWCNTs/RGO mixed-dimensional MCNCs displayed the improved impedance matching characteristics, conduction loss and polarization loss capabilities, which contributed to their enhanced EMWAPs. The as-prepared Fe_3O_4-$FeCO_3$/MWCNTs/RGO mixed-dimensional MCNCs simultaneously exhibited the good absorption ability, wide absorption bandwidth, thin matching thickness and low density. Consequently, this work provided a simple and propagable approach to synthesize magnetic MWCNTs/RGO-based mixed-dimensional MCNCs in high efficiency, which makes the best of interface and magnetic-dielectric synergy strategy for exploiting high-efficiency novel microwave absorbers.

2. Experimental section

2.1. Material

The used initial reagents in the experiment were analytical grade. Among them, hydroxylated MWCNTs were bought from Jiangsu XFNANO Material Technology CO., LTD. ($FeSO_4{\cdot}7H_2O$), urea [$CO(NH_2)_2$] and sodium hydroxide (NaOH) were obtained from Shanghai Aladdin Biochemical Technology CO., LTD, respectively.

2.2. Fabrication of Fe_3O_4-$FeCO_3$/MWCNTs/RGO mixed-dimensional MCNCs

Firstly, according to the previous work [31], few-layer GO was produced by a modified Hummers method. GO solution could be obtained by ultrasonic dissolving the prepared GO powder (60 mg) into deionized water (30 mL) at room temperature for ca. 30 min. Secondly, hydroxylated MWCNTs (30 mg) were added into the formed GO solution and sonicated for another 30 min to generate the MWCNTs/GO solution. Thirdly, $FeSO_4{\cdot}7H_2O$ (1.39 g) was placed into the MWCNTs/GO solution under the mechanical stirring with an electric mixer. And the pre-configured NaOH solution (5 mL, 2 M) was dropped into the abovementioned mixture and vigorously stirred for ca. 1 h. Subsequently, 3.2 g of $CO(NH_2)_2$ was placed into mixed solution and stirred for ca. 5 min. After that, the resulted solution was poured into a Teflon-lined stainless-steel (100 mL) for hydrothermal reaction at 180 °C for 12 h. Finally, the Fe_3O_4-$FeCO_3$/MWCNTs/RGO mixed-dimensional MCNCs named as FCRGO-1 was achieved after the repeatedly washed with anhydrous ethanol and deionized water, followed by magnetic centrifugation and freeze-drying. To adjust their EM properties, we modulated the amounts of GO and CNTs when the other experimental conditions kept unchangeable. Amongst, the Fe_3O_4-$FeCO_3$/MWCNTs/RGO mixed-dimensional MCNCs denoted as FCRGO-2 and FCRGO-3 could be produced when 80 mg of GO and 40 mg of MWCNTs, 100 mg of GO and 50 mg of MWCNTs were used as the precursors.

2.3. Characterization and measurement

To investigate the morphology, phase and chemical valence, the obtained Fe_3O_4-$FeCO_3$/MWCNTs/RGO mixed-dimensional MCNCs were characterized by X-ray powder diffractometer (XRD), X-ray Photoelectron spectroscopy (XPS), scanning electron microscope (SEM) and transmission electron microscope (TEM), respectively. In order to study the EM parameters and MAPs, 15 wt% of Fe_3O_4-$FeCO_3$/MWCNTs/RGO MCNCs and 85 wt% of paraffin were mixed and pressed into a toroidal shape with the external diameter of 7.00 mm and internal diameter of 3.00 mm. And the obtained cylindrical samples were measured over a vector network analyzer (R&S®ZNB-40). Based on and transmission line theory and EM parameters ($\varepsilon = \varepsilon' - j\varepsilon''$ and $\mu = \mu' - j\mu''$), the reflection loss (RL) values of samples were achieved by the following equations [32]:

$$Z_{in} = Z_0\sqrt{\frac{\mu}{\varepsilon}}\tanh\left(j\frac{2\pi fd\sqrt{\mu\varepsilon}}{c}\right) \quad (1)$$

$$RL = 20\log\left|\frac{Z_{in} - Z_0}{Z_{in} + Z_0}\right| \quad (2)$$

Where ε, μ, d, c, f, Z_0 and Z_{in} represent complex permittivity, complex permeability, thickness of sample, velocity of light, frequency of EM wave, impedance of air and input impedance of MAs, respectively.

3. Results and discussion

3.1. Microstructures and phases of Fe_3O_4-$FeCO_3$/MWCNTs/RGO mixed-dimensional MCNCs

Firstly, the microstructures of FCRGO samples were investigated by SEM. Fig. 1 gives the SEM images of FCRGO-1, FCRGO-2 and FCRGO-3 samples. As shown in Fig. 1a, one can see that the obtained FCRGO-1 sample exhibits a representative three-dimensional (3D) hierarchical structure, which is composed of 0D Fe_3O_4-$FeCO_3$ nanoparticles, 1D MWCNTs and 2D RGO nanosheets. The high-resolution SEM investigation (as presented in Fig. 1b and c) reveals that a large number of Fe_3O_4-$FeCO_3$ nanoparticles and MWCNTs are well attached to the surface of

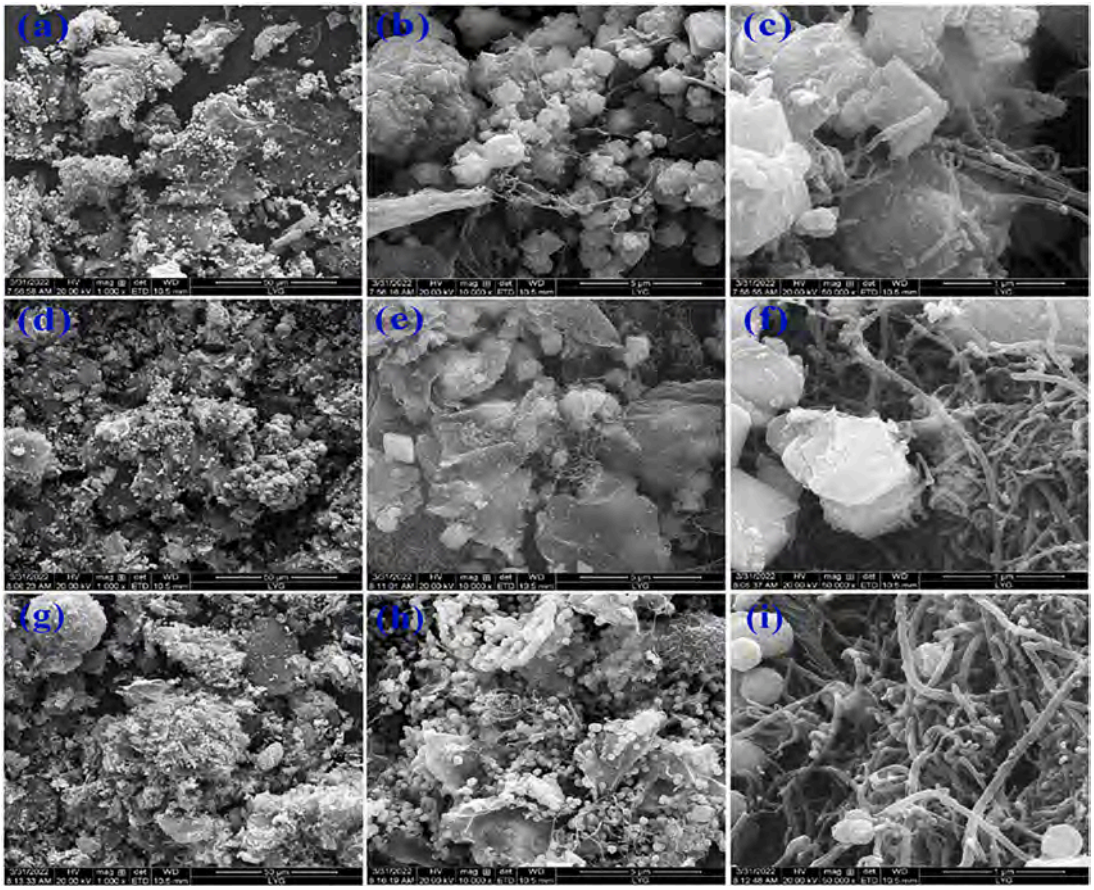

Fig. 1. SEM images of (a-c) FCRGO-1, (d-f) FCRGO-2 and (g-i) FCRGO-3, respectively.

RGO nanosheets. Likewise, similar to FCRGO-1, the SEM observations of FCRGO-2 (as displayed in Fig. 1d-f) and FCRGO-3 (as presented in Fig. 1 g-i) indicate that the obtained samples also consist of 1D MWCNTs, 0D Fe_3O_4-$FeCO_3$ nanoparticles and 2D sheet-like RGO, which collaborates the typical 3D hierarchical structures. By comparison, it can be found that the MWCNTs and RGO with progressively enhanced contents in the obtained FCRGO samples can be produced with increasing the amounts of MWCNTs and GO, which is very conducive to improve the interfaces and conductive performance. Similar to RGO—CNT-Co_3S_4 and CeO_2/GO/CNTs MCNCs reported elsewhere [33,34], the obtained results suggest that the obtained FCRGO samples consisting of 2D RGO, 1D MWCNTs and large quantities of 0D Fe_3O_4-$FeCO_3$ nanoparticles are synthesized in high efficiency and large scale via a facile hydrothermal and freeze-drying process.

To further confirm the microstructures, Fig. 2 gives the TEM images of as-prepared FCRGO samples. As shown in Fig. 2a, one can see that the as-prepared FCRGO-1 is a typical mixed-dimensional MCNCs, which includes 0D Fe_3O_4-$FeCO_3$ nanoparticles, 1D MWCNTs and 2D RGO nanosheets. The closer TEM investigation (as presented in Fig. 2b and c) reveal that massive Fe_3O_4-$FeCO_3$ nanoparticles (marked by the red arrow) are anchored on the surface of MWCNTs (labeled by the yellow arrow) and RGO (signed by the blue arrow), which effectively form a 3D conductive network. Same to FCRGO-1, the TEM observation reveals indicate that 2D RGO, 1D MWCNTs and 0D Fe_3O_4-$FeCO_3$ nanoparticles can be clearly observed in the obtained FCRGO-2 (shown in Fig. 2d-f) and FCRGO-3 (shown in Fig. 2 g-i). The results further confirm that the MWCNTs are well bound with the sheet-like RGO and Fe_3O_4-$FeCO_3$ nanoparticles are well attached on the outer surface of MWCNTs and RGO to form the 3D hierarchical mixed-dimensional networks. Furthermore, the comparison results further verify that the progressively enhanced content of MWCNTs and RGO can be observed in the as-prepared FCRGO samples with enhancing the qualities of MWCNTs and GO, which is accord with the experimental results and SEM investigations. In general, the SEM and TEM investigations demonstrate that the paper-like GO, MWCNTs and Fe_3O_4-$FeCO_3$ nanoparticles are mutually correlated to each other for the establishment of 3D hierarchical mixed-dimensional MCNCs.

Fig. 3 provides the XRD patterns, XPS spectra of the obtained FCRGO samples to detect their chemical compositions and phases. As shown in Fig. 3a, it can be found that the obtained FCRGO-1, FCRGO-2 and FCRGO-3 samples presents the similar XRD diffraction peaks, which indicates their similar phases. And the diffraction peaks at 62.55°, 56.96°, 43.07°, 35.44°, 30.09° and 18.29° can be assigned to (440), (511), (400), (311), (220) and (111) crystal faces of spinel Fe_3O_4 (JCPDS:85–1436). And there are four obvious characteristic peaks of 24.75°, 31.99°, 38.34° and 52.83° on the XRD pattern, which correspond to the (012), (104), (110) and (116) crystal planes of $FeCO_3$ (JCPDS: 29–0696), respectively. Similar to GO/CNT-Fe_3O_4 MCNCs [35], there are no characteristic XRD diffraction peaks assigned to RGO and MWCNTs, which is related to the inhibition of RGO restacking and the dispersion of Fe_3O_4-$FeCO_3$ with large quantities on the surface of RGO sheet and MWCNTs [36]. Furthermore, Raman spectroscopy was conducted to analyze the graphitization of carbon. As presented in Figure S1 (Supporting Information), the FCRGO samples display two characteristic peaks of carbon located at ca. 1340 cm^{-1} and 1570 cm^{-1}, which are referred to D-band and G-band, respectively. The Raman spectra confirm the existence of RGO and MWCNTs [25,37]. To verify the chemical valence, the as-prepared sample was characterized by the XPS. Taking FCRGO-2 as example, the XPS survey spectrum (as shown in Fig. 3b) has four distinct peaks belonged to the Fe $2p_{1/2}$, Fe $2p_{3/2}$, O 1 s and C 1 s, which originate from the elements of Fe, O and C. As marked in Fig. 3c, the high-resolution XPS spectrum of C 1 s can be deconvoluted into three

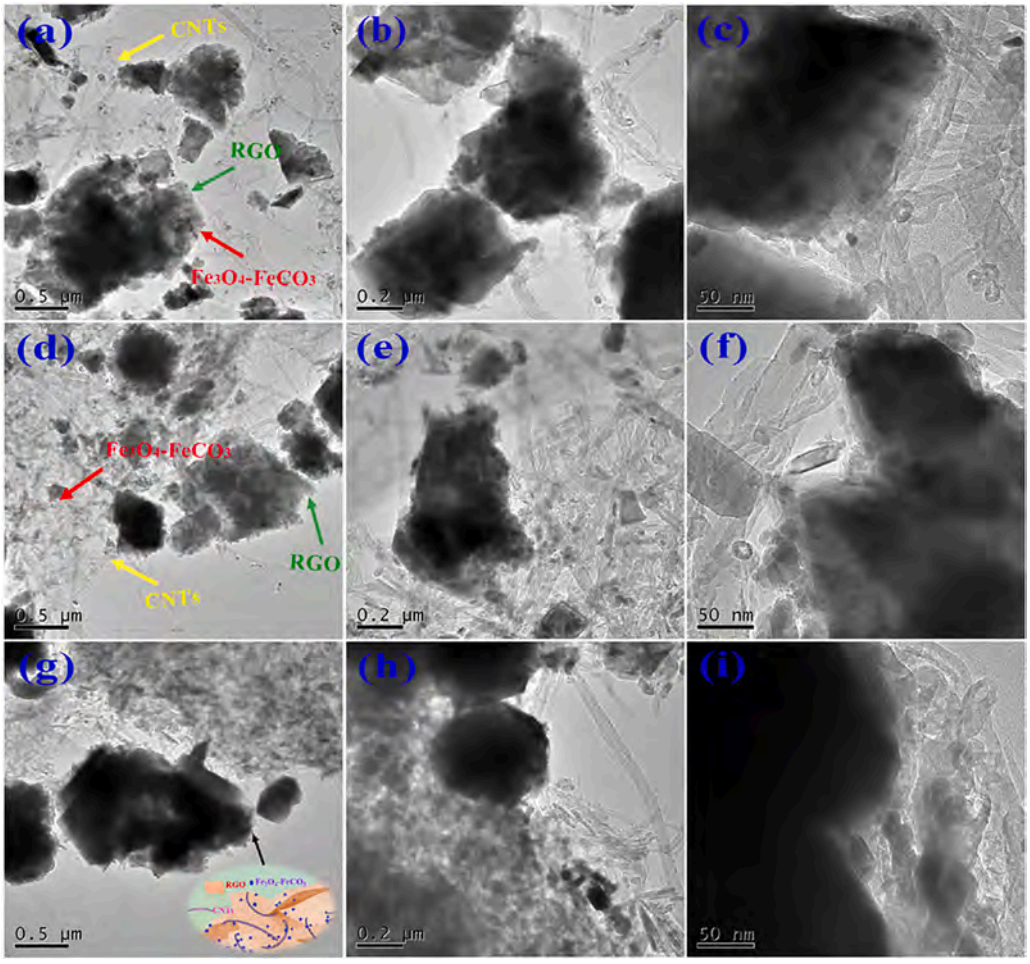

Fig. 2. Different resolutions of TEM images for (a-c) FCRGO-1, (d-f) FCRGO-2 and (g-i) FCRGO-3, respectively.

peaks at ca. 288.37 eV, 285.25 eV and 284.38 eV, which correspond to the different functional groups of C atoms including O—C = O, C—O/C = O and C—C/C = C, respectively [38,39]. Equally, as presented in Fig. 3d, the high resolution XPS spectrum of Fe 2p can be divided into four peaks including Fe $2p_{3/2}$, Fe $2p_{1/2}$ and their satellite peaks, which reveal the oxidation states of Fe^{2+} and Fe^{3+} in the obtained sample [40, 41]. Furthermore, the comparison XPS results (as shown in Figure S2) indicate that the obtained FCRGO-1 and FCRGO-3 exhibit the analogical XPS spectra, which implies their similar surface chemical compositions and valences. In general, the obtained SEM, TEM, XRD and XPS results reveal that mixed-dimensional Fe_3O_4-$FeCO_3$/MWCNTs/RGO MCNCs were produced in high efficiency by means of our proposed hydrothermal and freeze-drying process.

3.2. EM performances and EMWAPs of Fe_3O_4-$FeCO_3$/MWCNTs/RGO MCNCs

To evaluate the EMWAPs of Fe_3O_4-$FeCO_3$/MWCNTs/RGO MCNCs, Fig. 4 gives the complex permittivity, dielectric loss tangent ($\tan\delta_\varepsilon = \varepsilon''/\varepsilon'$) and RL values. In the light of Debye theory, the values of ε' and ε'' are expressed by the following formulas [42]:

$$\varepsilon' = \varepsilon_\infty + \frac{\varepsilon_s - \varepsilon_\infty}{1 + (2\pi f\tau)^2} \tag{3}$$

$$\varepsilon'' = \varepsilon''_p + \varepsilon''_c = \frac{\varepsilon_s - \varepsilon_\infty}{1 + (2\pi f\tau)^2} 2\pi f\tau + \frac{\sigma_{ac}}{2\pi f\varepsilon_0} \tag{4}$$

Where τ, ε''_p, ε''_c, ε_∞, σ_{ac} and ε_s are relaxation time, polarization loss, conductivity loss, relative dielectric permittivity at the infinite frequency limit, alternative conductivity and static permittivity, respectively. As shown in Fig. 4a, the FCRGO-1, FCRGO-2 and FCRGO-3 samples exhibit the decreased ε' values in the tested frequency region, which can be attributed to the increased value of frequency according to the Debye theory [43]. And their ε' values are in the range of 5.38–4.85, 5.90–5.28 and 10.01–6.38, respectively. One can find that their ε' values are as follows: FCRGO-1<FCRGO-2<FCRGO-3, which can be attributed to the enhanced content of high dielectric RGO and MWCNTs. Furthermore, one can find that the ε'' value (as presented in Fig. 4b) of FCRGO-1, FCRGO-2 and FCRGO-3 samples shows the enhancement trend when the frequency increases from 2.00 to 18.00 GHz. On basis of Eq. (3), the measured ε'' curves suggest the key role of polarization loss in the designed mixed-dimensional Fe_3O_4-$FeCO_3$/MWCNTs/RGO MCNCs [44]. Equally, the comparison results suggest the enhanced content of MWCNTs and RGO effectively boost their ε'' values, which favor the improvement of dielectric loss capability [45]. And the tunable EM parameters are very propitious to boost the impedance matching characteristic and EMWAPs [46]. As provided in Fig. 4c, we can find that the as-prepared Fe_3O_4-$FeCO_3$/MWCNTs/RGO mixed-dimensional MCNCs exhibit the progressively increased $\tan\delta_\varepsilon$ values with the enhanced contents of MWCNTs and RGO, which indicates their boosted dielectric loss abilities [47]. On basis of Eqs. (1), (2) and EM parameters (Figures 4a, 4b and S3), their RL values can be obtained. It can be observed that the minimum RL (RL_{min}) values for FCRGO-1, FCRGO-2 and FCRGO-3 samples (as given in Fig. 4d-f) are −55.89 dB at 12.36 GHz, −56.63 dB at 15.00 GHz and −46.11 dB at 11.00 GHz, respectively. And the matching thicknesses (d_m) values corresponding to RL_{min}

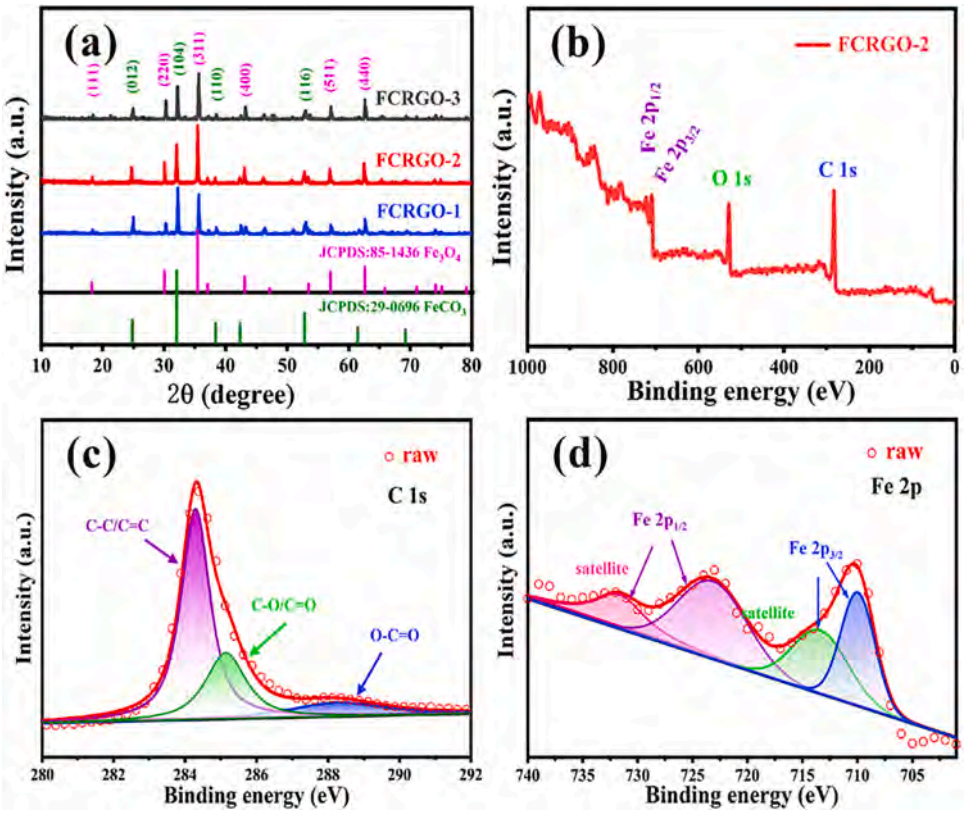

Fig. 3. (a) XRD patterns of FCRGO-1, FCRGO-2 and FCRGO-3. (b-d) XPS spectra of FCRGO-2.

values are 8.22 mm, 1.87 mm and 2.46 mm. Additionally, as presented in Fig. 4 g-i, the effective absorption bandwidth (EAB) values for FCRGO-1, FCRGO-2 and FCRGO-3 samples are 3.04 GHz (14.96–18.00 GHz) at 6.31 mm, 3.00 GHz (15.00–18.00 GHz) at 2.19 mm, and 6.20 GHz (11.80–18.00 GHz) at 1.99 mm, respectively. In general, it can be seen that the enhanced contents of MWCNTs and RGO effectively boost the comprehensive EMWAPs of designed mixed-dimensional Fe_3O_4-$FeCO_3$/MWCNTs/RGO samples. In particular, the obtained FCRGO-3 sample simultaneously exhibits the excellent performances including good absorption capability, large absorption bandwidth, low density, small matching thicknesses (~2 mm), etc. Additionally, as collected in Table 1, it can be seen that the obtained FCRGO samples can also be acted as the promising high efficiency MAs [48,49].

3.3. Analyses the difference in properties and main avenues of EM wave attenuation

Based on the obtained results, it is found that the enhanced contents of MWCNTs and RGO contribute to the enhanced comprehensive EMWAPs of designed mixed-dimensional Fe_3O_4-$FeCO_3$/MWCNTs/RGO samples. To find out the reasons, the EM wave attenuation and impedance matching characteristics including conductivity loss (ε''_c), polarization loss (ε''_p), attenuation constant (α) and impedance matching ratio (Z) were investigated in details, which were calculated based on the Debye theory [50]:

$$\alpha = \frac{\sqrt{2}\pi f}{c}\sqrt{(\mu''\varepsilon'' - \mu'\varepsilon') + \sqrt{(\mu''\varepsilon'' - \mu'\varepsilon')^2 + (\varepsilon'\mu'' + \varepsilon''\mu')^2}} \quad (5)$$

$$Z = |Z_{in} / Z_0| \quad (6)$$

Based on the Eqs. (3–6) and EM parameters, Fig. 5 provides the values of ε''_c, ε''_p, α and Z values of the obtained mixed-dimensional Fe_3O_4-$FeCO_3$/MWCNTs/RGO MCNCs. As shown in Fig. 5a and b, the obtained mixed-dimensional Fe_3O_4-$FeCO_3$/MWCNTs/RGO samples present the decreased enhanced ε''_c values and enhanced ε''_p values between 2.00 and 18.00 GHz, which are identical with the obtained ε'' values and Debye theory. By comparison, one can find that the ε''_c and ε''_p values are as follows: FCRGO-3>FCRGO-2>FCRGO-1, which means the gradually strengthened conductivity and polarization loss and capabilities [51]. And the increased ε''_c values root in the increased contents of RGO and MWCNTs, which greatly improves their conductivities [52]. And the increased ε''_p values are ascribed to the formation of much more interfaces amongst the generated 0D Fe_4O_3 nanoparticles, 1D MWCNTs and 2D sheet-like RGO in the designed mixed-dimensional Fe_3O_4-$FeCO_3$/MWCNTs/RGO samples, which can be verified by the aforementioned TEM and SEM investigations. Moreover, the designed mixed-dimensional Fe_3O_4-$FeCO_3$/MWCNTs/RGO MCNCs present much lower ε''_c values than the obtained ε''_p ones, which further confirms the main contribution of polarization loss [41]. As given in Fig. 5c, the obtained results suggest that the obtained Fe_3O_4-$FeCO_3$/MWCNTs/RGO samples present the boosted α values with increasing the amounts of GO and MWCNTs, which verify their boosted EM wave attenuation abilities [41,53]. Likewise, as the presented Fig. 5d-f, the obtained Z values reveal that the obtained FCRGO-3 exhibits the optimal impedance matching characteristic, and the obtained FCRGO-1 presents the worst one. Generally, the above results indicate that the generated abundant interface, increased contents of RGO and MWCNTs contribute to the superior conductivity loss, polarization loss, EM wave attenuation capabilities and impedance matching characteristics, which result in the strengthened EMWAPs of mixed-dimensional Fe_3O_4-$FeCO_3$/MWCNTs/RGO samples. And the outstanding EMWAPs of FCRGO-3 sample can be explained by its extraordinary impedance matching characteristic and interfacial effect.

To easily understand the excellent EMWAPs, Fig. 6 provides the main EM wave loss avenues of the designed mixed-dimensional Fe_3O_4-$FeCO_3$/MWCNTs/RGO MCNCs based on the achieved results and previously reported models [54,55]. And the main path of EM wave dissipation mainly roots in the following factors: (i) the designed

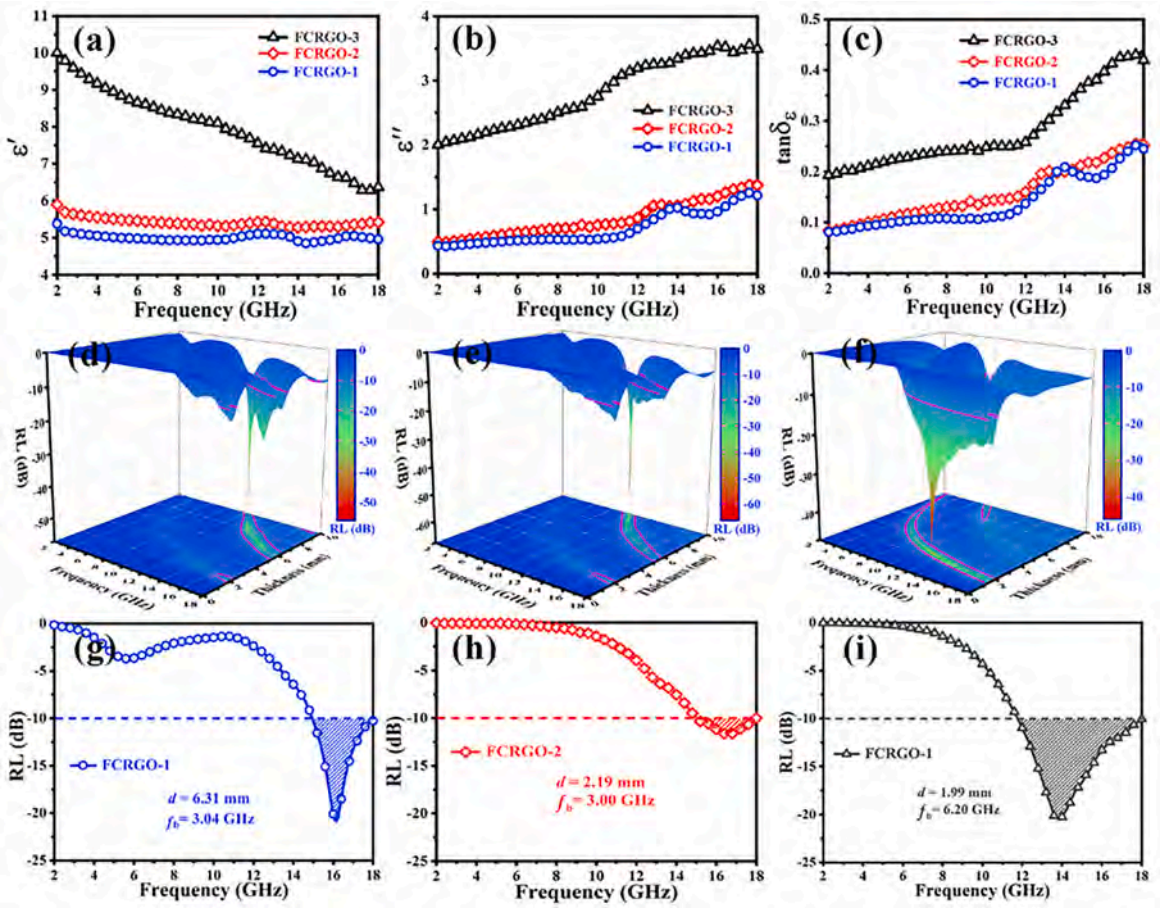

Fig. 4. (a) Real parts of complex permittivity, (b) imaginary parts of complex permittivity, (c) loss tangent, (d-f) 3D RL color maps, and (g-i) 2D RL curves of FCRGO-1, FCRGO-2 and FCRGO-3.

Table 1
Characteristic values about EMWAPs among the recently representative MCNCs.

Substances	EAB (GHz)	d_m (mm)	RL_{min} (dB)	d_m (mm)	References
$CoFe_2O_4$@ MCHS	2.40	5.00	−29.70	5.00	[7]
MoS_2@PEDOT/GO	6.48	2.20	−48.65	4.50	[9]
$ZnFe_2O_4$@MoS_2	5.20	1.88	−31.29	1.61	[10]
MoS_2@C	3.70	2.63	−62.30	2.88	[17]
Co/NC@MnO_2	6.20	2.10	−54.70	2.10	[20]
MoS_2/CoS_2/VN	5.76	2.02	−50.48	2.02	[21]
Fe_3O_4@$Ti_3C_2T_x$/CNTs	5.80	2.00	−40.10	2.00	[24]
HC@MoS_2	6.00	2.06	−42.63	1.92	[30]
CF/CNTs@Fe_3C@Fe_3O_4	5.00	1.81	−44.48	1.68	[31]
CoNi@void@C	5.20	1.95	−50.97	2.05	[33]
CP/Co	5.00	1.68	−52.71	1.65	[46]
PBHAC/MoS_2	6.08	2.00	−57.80	1.93	[48]
CoNi@Air@C/SiO_2@PPy	4.80	2.06	−52.75	2.72	[49]
FCRGO-3	6.20	1.99	−46.11	2.46	This work

mixed-dimensional Fe_3O_4-$FeCO_3$/MWCNTs/RGO MCNCs consisting of 2D RGO, 1D MWCNTs and a large number of Fe_4O_3 nanoparticles results in the formation of plentiful interfaces, which greatly aggrandize the interfacial polarization to dissipate the penetrated EM waves [56]. (ii) the obtained Fe_3O_4-$FeCO_3$/MWCNTs/RGO MCNCs consisting of Fe_3O_4-$FeCO_3$, MWCNTs and RGO can simultaneously provide the magnetic loss, dielectric loss and excellent synergistic effect, which contributes to the enhancement of EMWAPs [57]. (iii) the elaborately designed Fe_3O_4-$FeCO_3$/MWCNTs/RGO mixed-dimensional MCNCs consisting of 2D RGO and 1D MWCNTs form a typical conductive network, which effectively improves the conductive loss capability [58, 59]. (iv) large amounts of residual polar groups and/or defects existed in the RGO and MWCNTs contribute to the enhanced dipole polarizations, which also helps to attenuate the EMW [45,60].

4. Conclusion

In short, Fe_3O_4-$FeCO_3$/MWCNTs/RGO mixed-dimensional MCNCs were well-designed and successfully produced in large scale by the means of a simple hydrothermal and freeze-drying process. And the SEM and TEM investigations reveal that the obtained Fe_3O_4-$FeCO_3$/MWCNTs/RGO MCNCs were composed of 2D RGO, 1D MWCNTs and 0D Fe_3O_4-$FeCO_3$ nanoparticles, which were well combined to form a typical mixed-dimensional hierarchical network. Owing to the unique mixed-

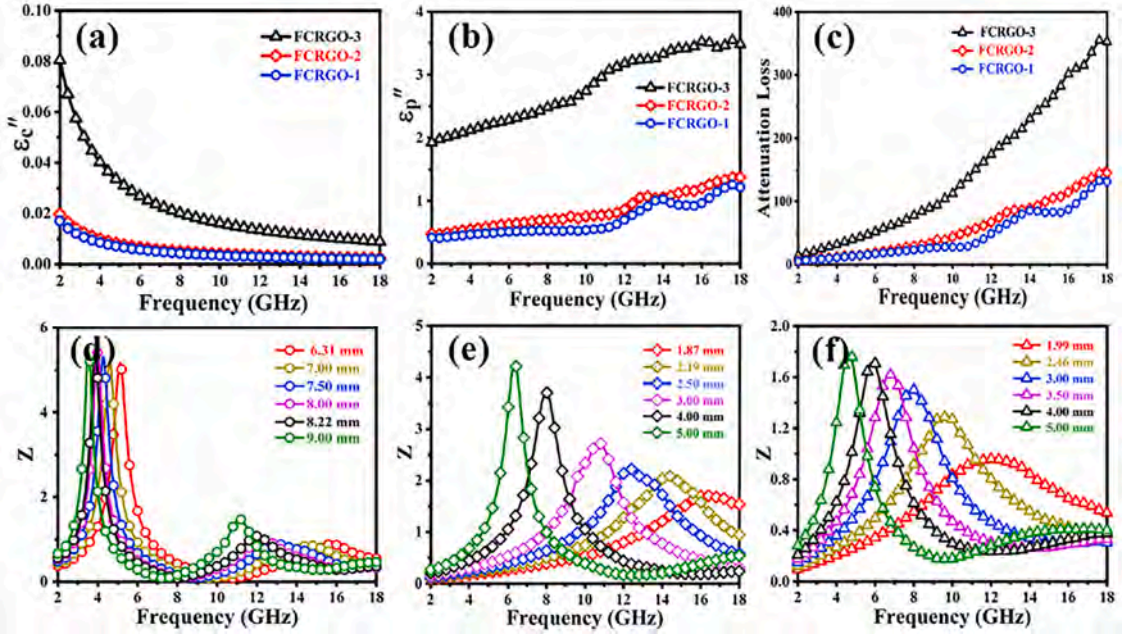

Fig. 5. (a) ε''_c, (b) ε''_p, (c) α, and (d-f) Z values of mixed-dimensional Fe_3O_4-$FeCO_3$/MWCNTs/RGO samples, respectively.

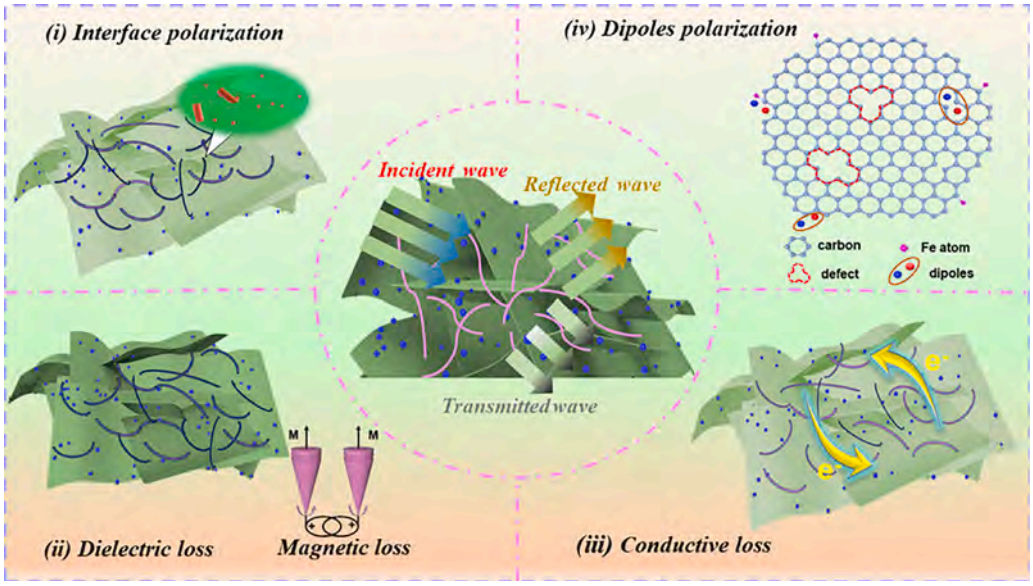

Fig. 6. Main path of EM wave attenuation for the designed mixed-dimensional Fe_3O_4-$FeCO_3$/MWCNTs/RGO MCNCs.

dimensional structure, abundant interfaces generated among RGO, MWCNTs and Fe_3O_4-$FeCO_3$ nanoparticles, which resulted in the excellent polarization loss capabilities. Furthermore, RGO and MWCNTs also contributed to their good conduction loss capabilities. And their impedance matching characteristics were effectively improved by regulating the amounts of GO and MWCNTs. Notably, the obtained FCRGO-3 sample achieved a RL_{min} value of −46.1 0 dB with the d_m of 2.46 mm and EAB value of 6.20 GHz with the d_m of 1.99 mm, which were ascribed to its excellent interfacial effect and impedance matching characteristic. Consequently, it was believed that this finding proposed an effective approach to fabricate high efficiency of mixed-dimensional magnetic MWCNTs/RGO-based MCNCs, which made best of impedance matching and interfacial strategy to optimize the EMWAPs.

CRediT authorship contribution statement

Hemin Wang: Investigation, Data curation, Writing – original draft. **Yanling Hao:** Visualization, Investigation, Data curation. **Lele Xiang:** Investigation, Data curation. **Xiaosi Qi:** Methodology, Visualization, Investigation, Writing – review & editing. **Lei Wang:** Data curation, Writing – review & editing. **Junfei Ding:** Data curation, Writing – review & editing. **Yunpeng Qu:** Visualization, Writing – review & editing. **Jing Xu:** Visualization, Writing – review & editing. **Wei Zhong:** Methodology, Writing – review & editing.

Declaration of Competing Interest

The authors declare that they have no known competing financial interests or personal relationships that could have appeared to influence

the work reported in this paper.

Data availability

No data was used for the research described in the article.

Acknowledgments

This work was supported by the Platform of Science and Technology and Talent Team Plan of Guizhou province (GCC [2023]007), Doctorial Start-up Fund of Guizhou University (2011–05), Fok Ying Tung Education Foundation (171095), Guizhou Provincial Basic Research Program (ZK [2021] 327) and National Natural Science Foundation of China (11964006 and 62105076) for financial support.

Supplementary materials

Supplementary material associated with this article can be found, in the online version, at doi:10.1016/j.materresbull.2023.112631.

References

[1] E.J. Bailey, K.I. Winey, Dynamics of polymer segments, polymer chains, and nanoparticles in polymer nanocomposite melts: a review, Prog. Polym. Sci. 105 (2020), 101242, https://doi.org/10.1016/j.progpolymsci.2020.101242.
[2] R. Liang, Y. Xue, X. Fu, A.N. Le, Q. Song, Y. Qiang, Q. Xie, R. Dong, Z. Sun, C. O. Osuji, J.A. Johnson, W. Li, M. Zhong, Hierarchically engineered nanostructures from compositionally anisotropic molecular building blocks, Nat. Mater. 21 (2022) 1434, https://doi.org/10.1038/s41563-022-01393-0.
[3] C.X. Wang, Y. Liu, Z.R. Jia, W.R. Zhao, G.L. Wu, Multicomponent nanoparticles synergistic one-dimensional nanofibers as heterostructure absorbers for tunable and efficient microwave absorption, Nano-Micro Lett. 15 (13) (2023), https://doi.org/10.1007/s40820-022-00986-3.
[4] W. Zhang, S.Y. Zhu, R. Luque, S. Han, L.Z. Hu, G.B. Xu, Recent development of carbon electrode materials and their bioanalytical and environmental applications, Chem. Soc. Rev. 45 (2016) 715–752, https://doi.org/10.1039/C5CS00297D.
[5] S. Bhattacharya, S.K. Samanta, Soft-Nanocomposites of nanoparticles and nanocarbons with supramolecular and polymer gels and their applications, Chem. Rev. 116 (2016) 11967–12028, https://doi.org/10.1021/acs.chemrev.6b00221.
[6] F.R. Baptista, S.A. Belhout, S. Giordani, S.J. Quinn, Recent developments in carbon nanomaterial sensors, Chem. Soc. Rev. 44 (2015) 4433–4453, https://doi.org/10.1039/C4CS00379A.
[7] L.G. Ren, Y.Q. Wang, X. Zhang, Q.C. He, G.L. Wu, Efficient microwave absorption achieved through in situ construction of core-shell $CoFe_2O_4$@mesoporous carbon hollow spheres, Int. J. Miner. Metall. 30 (2023) 504–514, https://doi.org/10.1007/s12613-022-2509-1.
[8] Y.Y. Guo, K.P. Ruan, G.S. Wang, J.W. Gu, Advances and mechanisms in polymer composites toward thermal conduction and electromagnetic wave absorption, Sci. Bull. 68 (2023) 1195–1212, https://doi.org/10.1016/j.scib.2023.04.036.
[9] S.J. Zhang, Y.X. Pei, Z.W. Zhao, C.L. Guan, G.L. Wu, Simultaneous manipulation of polarization relaxation and conductivity toward self-repairing reduced graphene oxide based ternary hybrids for efficient electromagnetic wave absorption, J. Colloid Interface Sci. 630 (2023) 453–464, https://doi.org/10.1016/j.jcis.2022.09.149.
[10] J.X. Xiao, X.S. Qi, X. Gong, Q. Peng, Y.L. Chen, R. Xie, W. Zhong, Tunable and improved microwave absorption of flower-like core@shell MFe_2O_4@MoS_2 (M = Mn, Ni and Zn) nanocomposites by defect and interface engineering, J. Mater. Sci. Technol. 139 (2023) 137–146, https://doi.org/10.1016/j.jmst.2022.08.022.
[11] B.L. Wang, Q. Wu, Y.G. Fu, T. Liu, A review on carbon/magnetic metal composites for microwave absorption, J. Mater. Sci. Technol. 86 (2021) 91–109, https://doi.org/10.1016/j.jmst.2020.12.078.
[12] X.H. Liang, Z.M. Man, B. Quan, J. Zheng, W.H. Gu, Z. Zhang, G.B. Ji, Environment-Stable Co_xNi_y encapsulation in stacked porous carbon nanosheets for enhanced microwave absorption, Nano-Micro Lett. 12 (2020) 102, https://doi.org/10.1007/s40820-020-00432-2.
[13] Y.C. Rao, X.S. Qi, Q. Peng, Y.L. Chen, X. Gong, R. Xie, W. Zhong, Flower-like NiO to flower-like NiO/Ni@C microspheres: an effective strategy to comprehensively improve the loss capabilities, J. Colloid Interf. Sci. 629 (2023) 981–993, https://doi.org/10.1016/j.jcis.2022.09.027.
[14] L.Y. Liang, Q.M. Li, X. Yan, Y.Z. Feng, Y.M. Wang, H.B. Zhang, X.P. Zhou, C.T. Liu, C.Y. Shen, X.L. Xie, Multifunctional magnetic $Ti_3C_2T_x$ MXene/Graphene aerogel with superior electromagnetic wave absorption performance, ACS Nano 15 (2021) 6622–6632, https://doi.org/10.1021/acsnano.0c09982.
[15] F. Zhang, S.Y. Yin, Y.F. Chen, Q. Zheng, L.J. Wang, W. Jiang, Ligand-directed construction of CNTs-decorated metal carbide/carbon composites for ultra-strong and broad electromagnetic wave absorption, Chem. Eng. J. 433 (2022), 133586, https://doi.org/10.1016/j.cej.2021.133586.
[16] J. Liu, J.Q. Tao, L.L. Gao, X.X. He, B. Wei, Y.S. Gu, Z.J. Yao, J.T. Zhou, Morphology-size synergy strategy of SiC@C nanoparticles towards lightweight and efficient microwave absorption, Chem. Eng. J. 433 (2022), 134484, https://doi.org/10.1016/j.cej.2021.134484.
[17] J. Zhao, Z. Gu, Q.G. Zhang, Stacking MoS_2 flower-like microspheres on pomelo peels-derived porous carbon nanosheets for high-efficient X-band electromagnetic wave absorption, Nano Res. (2023), https://doi.org/10.1007/s12274-023-6090-3.
[18] L.L. Liang, W.H. Gu, Y. Wu, B.S. Zhang, G.H. Wang, Y. Yang, G.B. Ji, Heterointerface engineering in electromagnetic absorbers: new insights and opportunities, Adv. Mater., 34 (2022) 2106195, https://doi.org/10.1002/adma.202106195.
[19] S.J. Zhang, Z.G. Gao, Z.B. Sun, B. Cheng, Z.W. Zhao, Y.C. Jia, G.L. Wu, Solid solution strategy for bimetallic metal-polyphenolic networks deriving electromagnetic wave absorbers with regulated heterointerfaces, Appl. Surf. Sci. 611 (2023), 155707, https://doi.org/10.1016/j.apsusc.2022.155707.
[20] C.H. Wei, M.K. He, M.Q. Li, X. Ma, W.L. Dang, P.B. Liu, J.W. Gu, Hollow Co/NC@MnO_2polyhedrons with enhanced synergistic effect for high-efficiency microwave absorption, Mater. Today Phys. (2023), 101142, https://doi.org/10.1016/j.mtphys.2023.101142.
[21] J.X. Zhou, D. Lan, F. Zhang, Y.H. Cheng, Z.R. Jia, G.L. Wu, P.F. Yin, Self-Assembled MoS_2 cladding for corrosion resistant and frequency-modulated electromagnetic wave absorption materials from X-band to Ku-band, Small (2023), https://doi.org/10.1002/smll.202304932.
[22] L. Kong, S.H. Luo, S.Y. Zhang, G.Q. Zhang, Y. Liang, Ultralight pyrolytic carbon foam reinforced with amorphous carbon nanotubes for broadband electromagnetic absorption, Int. J. Miner. Metall. 30 (2023) 570–580, https://doi.org/10.1007/s12613-022-2476-6.
[23] X.L. Cao, Z.R. Jia, D.Q. Hu, G.L. Wu, Synergistic construction of three-dimensional conductive network and double heterointerface polarization via magnetic FeNi for broadband microwave absorption, Adv. Compos. Hybrid Mater. 5 (2022) 1030–1043, https://doi.org/10.1007/s42114-021-00415-w.
[24] C. Zhang, Z.C. Wu, C.Y. Xu, B.T. Yang, L. Wang, W.B. You, R.C. Che, Hierarchical $Ti_3C_2T_x$ MXene/Carbon nanotubes hollow microsphere with confined magnetic nanospheres for broadband microwave absorption, Small 18 (2022), 2104380, https://doi.org/10.1002/smll.202104380.
[25] X.Y. Fu, Q. Zheng, L. Li, M.S. Cao, Vertically implanting $MoSe_2$ nanosheets on the RGO sheets towards excellent multi-band microwave absorption, Carbon N Y 197 (2022) 324–333, https://doi.org/10.1016/j.carbon.2022.06.037.
[26] D.Q. Zhang, T.T. Liu, J.Y. Cheng, Q. Cao, G.P. Zheng, S. Liang, H. Wang, M.S. Cao, Lightweight and high-performance microwave absorber based on 2D WS_2-RGO heterostructures, Nano-Micro Lett. 11 (2019) 38, https://doi.org/10.1007/s40820-019-0270-4.
[27] S. Zhang, X.H. Liu, C.Y. Jia, Z.S. Sun, H.W. Jiang, Z.R. Jia, G.L. Wu, Integration of multiple heterointerfaces in a hierarchical 0D@2D@1D structure for lightweight, flexible, and hydrophobic multifunctional electromagnetic protective fabrics, Nano-micro Lett. 15 (2023) 204, https://doi.org/10.1007/s40820-023-01179-2.
[28] Y. Sun, W. Zhong, Y.Q. Wang, X.B. Xu, T.T. Wang, L.Q. Wu, Y.W. Du, MoS_2-Based mixed-dimensional van der waals heterostructures: a new platform for excellent and controllable microwave-absorption performance, ACS Appl. Mater. Interfaces 9 (2017) 34243–34255, https://doi.org/10.1021/acsami.7b10114.
[29] X.J. Xiao, X.S. Qi, X. Gong, Y.L. Chen, R. Xie, W. Zhong, Defect and interface engineering in core@shell structure hollow carbon@MoS_2 nanocomposites for boosted microwave absorption performance, Nano Res. 15 (2022) 7778–7787, https://doi.org/10.1007/s12274-022-4625-7.
[30] T.M. Jia, X.S. Qi, L. Wang, J.L. Yang, X. Gong, Y.L. Chen, Y.P. Qu, Q. Peng, W. Zhong, Constructing mixed-dimensional lightweight flexible carbon foam/carbon nanotubes-based heterostructures: an effective strategy to achieve tunable and boosted microwave absorption, Carbon N Y 206 (2023) 364–374, https://doi.org/10.1016/j.carbon.2023.02.046.
[31] X.N. Tang, C.Z. Liu, X.R. Chen, Y.Q. Deng, X.H. Chen, J.J. Shao, Q.H. Yang, Graphene aerogel derived by purification-free graphite oxide for high performance supercapacitor electrodes, Carbon N Y 146 (2019) 147–154, https://doi.org/10.1016/j.carbon.2019.01.096.
[32] C. Li, X.S. Qi, X. Gong, Q. Peng, Y.L. Chen, R. Xie, W. Zhong, Magnetic-dielectric synergy and interfacial engineering to design yolk–shell structured CoNi@void@C and CoNi@void@C@MoS_2 nanocomposites with tunable and strong wideband microwave absorption, Nano Res. 15 (2022) 6761–6771, https://doi.org/10.1007/s12274-022-4468-2.
[33] A. Mohammadi, N. Arsalani, A.G. Tabrizi, S.E. Moosavifard, Z. Naqshbandi, L. S. Ghadimi, Engineering rGO-CNT wrapped Co_3S_4 nanocomposites for high-performance asymmetric supercapacitors, Chem. Eng. J. 334 (2018) 66–80, https://doi.org/10.1016/j.cej.2017.10.029.
[34] C.Y. Min, Z.B. He, H.J. Song, D.D. Liu, W. Jia, J.M. Qian, Y.H. Jin, L. Guo, Fabrication of novel CeO_2/GO/CNTs ternary nanocomposites with enhanced tribological performance, Appl. Sci. 9 (2019) 170, https://doi.org/10.3390/app9010170.
[35] S.J. Yan, L.N. Wang, T.H. Wang, L.Q. Zhang, Y.F. Li, S.L. Dai, Synthesis and microwave absorption property of graphene oxide/carbon nanotubes modified with cauliflower-like Fe_3O_4 nanospheres, Appl. Phys. A 122 (2016) 235, https://doi.org/10.1007/s00339-016-9769-4.
[36] L. Wang, X.L. Jia, Y.F. Li, F. Yang, L.Q. Zhang, L.P. Liu, X. Ren, H.T. Yang, Synthesis and microwave absorption property of flexible magnetic film based on graphene oxide/carbon nanotubes and Fe_3O_4 nanoparticles, J. Mater. Chem. A 2 (2014) 14940–14946, https://doi.org/10.1039/C4TA02815E.
[37] X.H. Huan, H.T. Wang, W.C. Deng, J.Q. Yan, K. Xu, H.B. Geng, X.D. Guo, X.L. Jia, J. S. Zhou, X.P. Yang, Integrating multi-heterointerfaces in a 1D@2D@1D

hierarchical structure via autocatalytic pyrolysis for Ultra-Efficient microwave absorption performance, Small 18 (2022), 2105411, https://doi.org/10.1002/smll.202105411.
[38] C.J. Shuai, F. Yang, Y. Shuai, S.P. Peng, S.J. Chen, Y.W. Deng, P. Feng, Silicon dioxide nanoparticles decorated on graphene oxide nanosheets and their application in poly(l-lactic acid) scaffold, J. Adv. Res. 48 (2023) 175–190, https://doi.org/10.1016/j.jare.2022.08.017.
[39] R. Mohammadkhani, M. Ramezanzadeh, S. Saadatmandi, B. Ramezanzadeh, Designing a dual-functional epoxy composite system with self-healing/barrier anti-corrosion performance using graphene oxide nano-scale platforms decorated with zinc doped-conductive polypyrrole nanoparticles with great environmental stability and non-toxicity, Chem. Eng. J. 382 (2020), 122819, https://doi.org/10.1016/j.cej.2019.122819.
[40] H. Alamgholiloo, N.N. Pesyan, R. Mohammadi, S. Rostamnia, M. Shokouhimehr, Synergistic advanced oxidation process for the fast degradation of ciprofloxacin antibiotics using a GO/CuMOF-magnetic ternary nanocomposite, J. Environ. Chem. Eng. 9 (2021), 105486, https://doi.org/10.1016/j.jece.2021.105486.
[41] N. Wang, Y. Wang, Z. Lu, R.R. Cheng, L.Q. Yang, Y.F. Li, Hierarchical core-shell FeS_2/Fe_7S_8@C microspheres embedded into interconnected graphene framework for high-efficiency microwave attenuation, Carbon N Y 202 (2023) 254–264, https://doi.org/10.1016/j.carbon.2022.10.083.
[42] Y.P. Qu, H.K. Wu, P.T. Xie, M. Zeng, Y.L. Chen, X. Gong, J.L. Yang, Q. Peng, Y. Xie, X.S. Qi, Carbon nanotube-carbon black/$CaCu_3Ti_4O_{12}$ ternary metacomposites with tunable negative permittivity and thermal conductivity fabricated by spark plasma sintering, Rare Met. (2023), https://doi.org/10.1007/s12598-023-02346-5.
[43] J.W. Wang, B.B. Wang, Z. Wang, L. Chen, C.H. Gao, B.H. Xu, Z.R. Jia, J.L. Wu, Synthesis of 3D flower-like ZnO/$ZnCo_2O_4$ composites with the heterogeneous interface for excellent electromagnetic wave absorption properties, J. Colloid Interface Sci. 586 (2021) 479–490, https://doi.org/10.1016/j.jcis.2020.10.111.
[44] X.G. Huang, J.W. Wei, Y.K. Zhang, B.B. Qian, Q. Jia, J. Liu, X.J. Zhao, G.F. Shao, Ultralight magnetic and dielectric aerogels achieved by metal-organic framework initiated gelation of graphene oxide for enhanced microwave absorption, Nano-Micro Lett. 14 (2022) 104, https://doi.org/10.1007/s40820-022-00851-3.
[45] K.Y. Cao, X. Yang, R. Zhao, W.D. Xue, Fabrication of an ultralight Ni-MOF-rGO aerogel with both dielectric and magnetic performances for enhanced microwave absorption: microspheres with hollow structure grow onto the GO nanosheets, ACS Appl. Mater. Interfaces 15 (2023) 9685–9696, https://doi.org/10.1021/acsami.2c22935.
[46] L.L. Xiang, X.S. Qi, Y.C. Rao, L. Wang, X. Gong, Y.L. Chen, Q. Peng, W. Zhong, A simple strategy to develop heterostructured carbon paper/Co nanoparticles composites with lightweight, tunable and broadband microwave absorption, Mater. Today Phys. 34 (2023), 101030, https://doi.org/10.1016/j.mtphys.2023.101030.
[47] J.F. Qiu, H.P. Cao, J. Liao, R.X. Du, K. Dou, N. Tsidaeva, W. Wang, 3D porous coral-like $Co_{1.29}Ni_{1.71}O_4$ microspheres embedded into reduced graphene oxide aerogels with lightweight and broadband microwave absorption, J. Colliod Interface Sci. 609 (2022) 12–22, https://doi.org/10.1016/j.jcis.2021.11.176.
[48] J. Li, Q.Q. Zhu, J.H. Zhu, Y.H. Cheng, Z.R. Jia, F. Lu, C. Wang, G.L. Wu, InimiTable 3D pyrolytic branched hollow architecture with multi-scale conductive network for microwave absorption, J. Mater. Sci. Technol. 173 (2024) 170–180, https://doi.org/10.1016/j.jmst.2023.06.066.
[49] Q.Q. Liang, L. Wang, X.S. Qi, Q. Peng, X. Gong, Y.L. Chen, R. Xie, W. Zhong, Hierarchical engineering of CoNi@Air@C/SiO_2@polypyrrole multicomponent nanocubes to improve the dielectric loss capability and magnetic-dielectric synergy, J. Mater. Sci. Technol. 147 (2023) 37–46, https://doi.org/10.1016/j.jmst.2022.10.069.
[50] Y.L. Wu, D. Lan, J.W. Ren, S.J. Zhang, A mini review of MOFs derived multifunctional absorbents: from perspective of components regulation, Mater. Today Phys. 36 (2023), 101178, https://doi.org/10.1016/j.mtphys.2023.101178.
[51] L.Q. Yang, Y. Wang, Z. Lu, R.R. Cheng, N. Wang, Y.F. Li, Construction of multi-dimensional NiCo/C/CNT/rGO aerogel by MOF derivative for efficient microwave absorption, Carbon N Y 205 (2023) 411–421, https://doi.org/10.1016/j.carbon.2023.01.057.
[52] Y. Wu, Y. Zhao, M. Zhou, S.J. Tan, R. Peymanfar, B. Aslibeiki, G.B. Ji, Ultrabroad microwave absorption ability and infrared stealth property of Nano-Micro CuS@rGO lightweight aerogels, Nano-Micro Lett. 14 (2022) 171, https://doi.org/10.1007/s40820-022-00906-5.
[53] D. Lan, Y. Wang, Y.Y. Wang, X.F. Zhu, H.F. Li, X.M. Guo, J.N. Ren, Z.H. Guo, G. L. Wu, Impact mechanisms of aggregation state regulation strategies on the microwave absorption properties of flexible polyaniline, J. Colloid Interface Sci. 651 (2023) 494–503, https://doi.org/10.1016/j.jcis.2023.08.019.
[54] Y.X. Han, M.K. He, J.W. Hu, P.B. Liu, Z.W. Liu, Z.L. Ma, W.B. Ju, J.W. Gu, Hierarchical design of FeCo-based microchains for enhanced microwave absorption in C band, Nano Res. 16 (2023) 1773–1778, https://doi.org/10.1007/s12274-022-5111-y.
[55] X.Y. Wang, T. Zhu, S.C. Chang, Y.K. Lu, W.B. Mi, W. Wang, 3D nest-like architecture of core-shell $CoFe_2O_4$@1T/2H-MoS_2 composites with tunable microwave absorption performance, ACS Appl. Mater. Interfaces 12 (2020) 11252–11264. https://pubs.acs.org/doi/10.1021/acsami.9b23489.
[56] X. Meng, W.J. Lei, W.W. Yang, Y.Q. Liu, Y.S. Yu, Fe_3O_4 nanoparticles coated with ultra-thin carbon layer for polarization-controlled microwave absorption performance,, J. Colloid Interf. Sci. 600 (2021) 382–389, https://doi.org/10.1016/j.jcis.2021.05.055.
[57] X.T. Chen, Y. Wu, W.H. Gu, M. Zhou, S.L. Tang, J.M. Cao, Zou Z.Q, G.B. Ji, Research progress on nanostructure design and composition regulation of carbon spheres for the microwave absorption, Carbon N Y 189 (2022) 617–633, https://doi.org/10.1016/j.carbon.2021.12.100.
[58] P.B. Liu, Y. Wang, G.Z. Zhang, Y. Huang, R.X. Zhang, X.H. Liu, X.F. Zhang, R. C. Che, Hierarchical engineering of double-shelled nanotubes toward hetero-interfaces induced polarization and microscale magnetic interaction, Adv. Funct. Mater. 32 (2022), 2202588, https://doi.org/10.1002/adfm.202202588.
[59] Z.R. Jia, D. Lan, M. Chang, Y. Han, G.L. Wu, Heterogeneous interfaces and 3D foam structures synergize to build superior electromagnetic wave absorbers, Mater. Today Phys. 37 (2023), 101215, https://doi.org/10.1016/j.mtphys.2023.101215.
[60] P.B. Liu, G.Z. Zhang, H.X. Xu, S.C. Cheng, Y. Huang, B. Ouyang, Y.T. Qian, R. X. Zhang, R.C. Che, Synergistic dielectric–magnetic enhancement via phase-evolution engineering and dynamic magnetic resonance, Adv. Funct. Mater. 33 (2023), 2211298, https://doi.org/10.1002/adfm.202211298.